Extension of self-seeding scheme with single crystal monochromator to lower energy < 5 keV as a way to generate multi-TW scale pulses at the European XFEL

Gianluca Geloni, [a,1] Vitali Kocharyan [b] and Evgeni Saldin [b]

[a] *European XFEL GmbH, Hamburg, Germany*

[b] *Deutsches Elektronen-Synchrotron (DESY), Hamburg, Germany*

Abstract

We propose a use of the self-seeding scheme with single crystal monochromator to produce high power, fully-coherent pulses for applications at a dedicated bio-imaging beamline at the European X-ray FEL in the photon energy range between 3.5 keV and 5 keV. We exploit the C(111) Bragg reflection (π-polarization) in diamond crystals with a thickness of 0.1 mm, and we show that, by tapering the 40 cells of the SASE3 type undulator the FEL power can reach up to 2 TW in the entire photon energy range. The present design assumes the use of a nominal electron bunch with charge 0.1 nC at nominal electron beam energy 17.5 GeV. The main application of the scheme proposed in this work is for single shot imaging of individual protein molecules.

1 Introduction

Despite the unprecedented increase in peak power of X-ray pulses from SASE X-ray FELs, some applications including imaging of complex molecules like proteins and other biologically interesting structures may still require higher photon flux (see, among others, [1]-[3]). The most promising way to extract more FEL power than that at saturation is by tapering the magnetic field of the undulator [4]-[7]. Also, a significant increase in power is achievable by starting the FEL process from monochromatic seed rather than from noise [8]-[10]. Self-seeding is a promising approach to significantly narrow

[1] Corresponding Author. E-mail address: gianluca.geloni@xfel.eu

the SASE bandwidth and to produce nearly transform-limited pulses [11]-[17]. The combination of self-seeding and tapering techniques would allow to meet the desired TW-scale output power for bio-imaging applications [18]-[22].

We recently proposed a study for a possible dedicated bio-imaging beamline at the European XFEL [23]. In that concept we suggested that the use of a single crystal self-seeding scheme would allow to deliver nearly transform-limited TW-scale X-ray pulses in the photon energy range between 8 keV and 13 keV. However, potential users of such a bio-imaging beamline mainly wish to investigate their samples in the energy range between 3 keV and 5 keV, where the diffraction signal is stronger. Finding a solution suitable for this spectral range is major challenge for self-seeding designers. In fact, due to high absorption, both single crystal monochromators and grating monochromators have a low throughput in the energy range between 3 keV and 5 keV. In [23] we proposed a method to get around this obstacle, which is based in essence on a fresh bunch technique [24] and exploits a conservative design of a self-seeding setup based on grating monochromator [25, 26] in the photon energy range between 0.3 keV and 1.7 keV.

In this work we propose an alternative possibility to provide bio-imaging capabilities in the photon energy range between 3 keV and 5 keV, based on an extension of the original design of the self-seeding scheme with single crystal monochromator down to 3 keV. We still suggest to use a diamond crystal with thickness 0.1 mm. However, we consider a symmetric C(111) Bragg reflection (π-polarization). This reflection will allow to cover the photon energy range from 3.5 keV to 5 keV. We demonstrate that the previously mentioned drawback of a low throughput can be overcome by enabling a cascade self-seeding scheme [27].

In its simplest configuration, a self-seeded XFEL consists of an input undulator and an output undulator separated by a single crystal monochromator. At photon energies below 5 keV absorption in crystals is very high and the simplest configuration, based on two undulators, is not optimal. A possible extension is to use a setup with three or more undulators separated by monochromators. Each cascade consists of an undulator acting as an amplifier, and of a single crystal monochromator. The amplification-monochromatization cascade scheme is distinguished, in performance, by a high signal-to-noise ratio and by small electron beam perturbations at the entrance of the output undulator. In this paper we study such scheme, which consists of two parts: first, a a succession of two amplification-monochromatization cascades and, second, an output undulator in which the monochromatic seed is amplified up to 2 TW power.

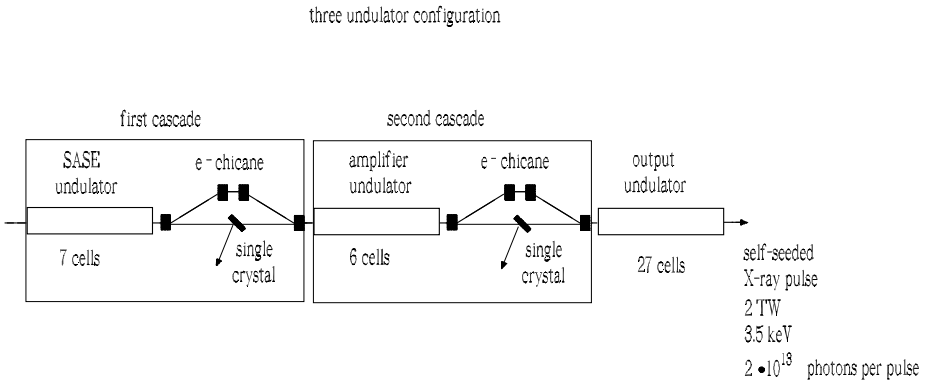

Fig. 1. Schematic of a two-cascade self-seeding scheme with single crystal monochromators. This scheme holds a great promise as a source of X-ray radiation in the 3.5 keV - 5 keV photon energy range for applications such as single biomolecule imaging.

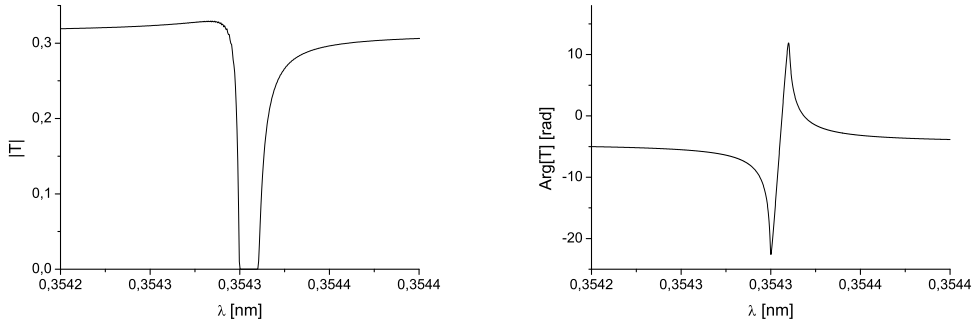

Fig. 2. Absolute value and phase of the transmission function pertaining the C(111) forward diffraction of a 100 μm-thick diamond crystal (π-polarization).

2 Principle of cascade self-seeding technique based on the use of single crystal monochromators

The self-seeding technique considered in this work is based on the substitution of a single undulator module with a weak chicane and a single crystal. Two cascades can be arranged sequentially as shown in Fig. 1.

The first undulator in Fig. 1 operates in the linear high-gain regime starting from the shot-noise in the electron beam. After the first undulator, the output SASE radiation passes through the monochromator, which reduces the bandwidth to the desired value. According to the wake monochromator principle, the SASE pulse coming from the first undulator impinges on a crystal set for Bragg diffraction.

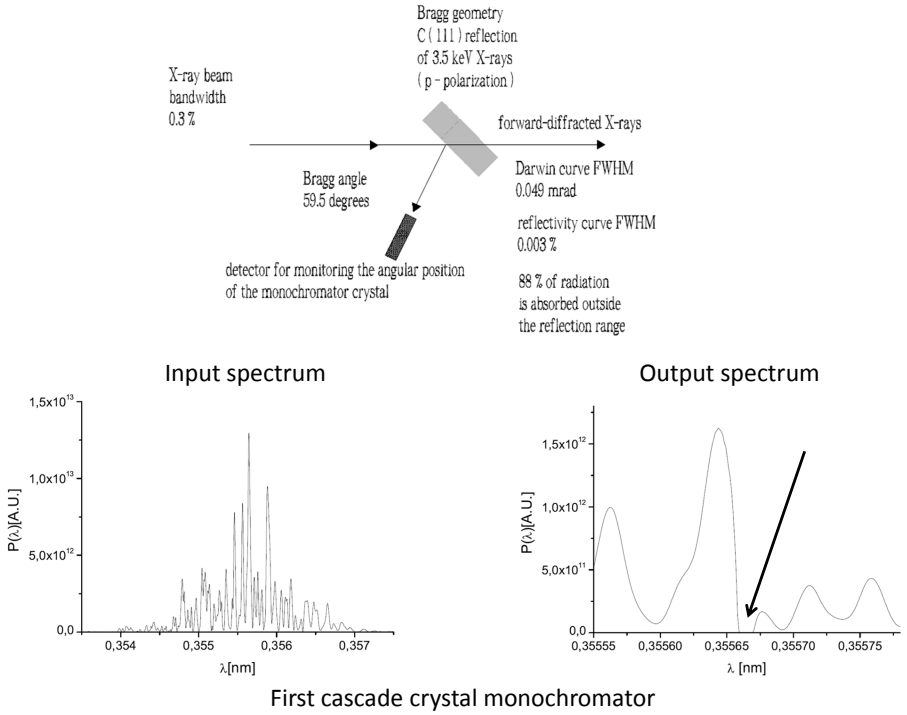

Fig. 3. Effect of the filtering process provided by the first diamond crystal on the incident spectrum of the radiation.

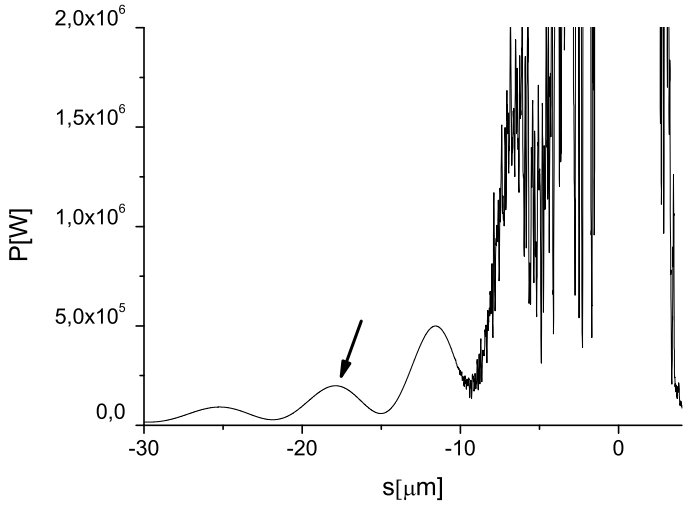

Fig. 4. Temporal shape of the seed signal from the first self-seeding setup. The black arrow indicates the seeding region used in this article.

The single crystal in Bragg geometry actually operates as a bandstop filter for the transmitted X-ray SASE radiation pulse. The filter transmission function in modulus and phase is shown in Fig. 2, where the central bandwidth can be tuned by properly tilting the crystal. In Fig. 3 we show the effect of the filtering through the crystal on the incident spectrum of the radiation. When

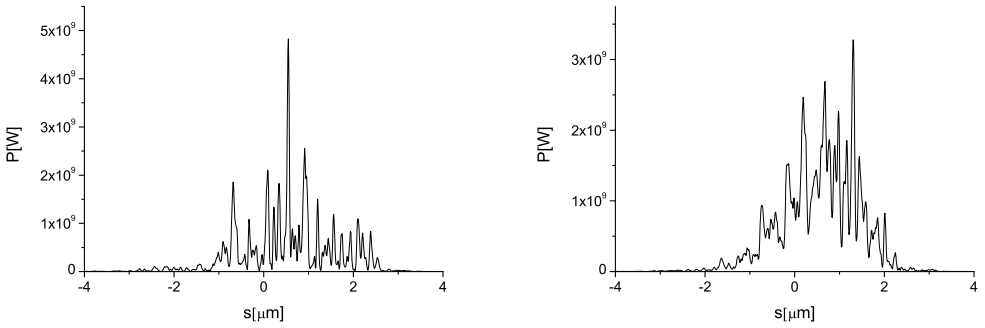

Fig. 5. Power before the first (left) and the second (right) monochromator.

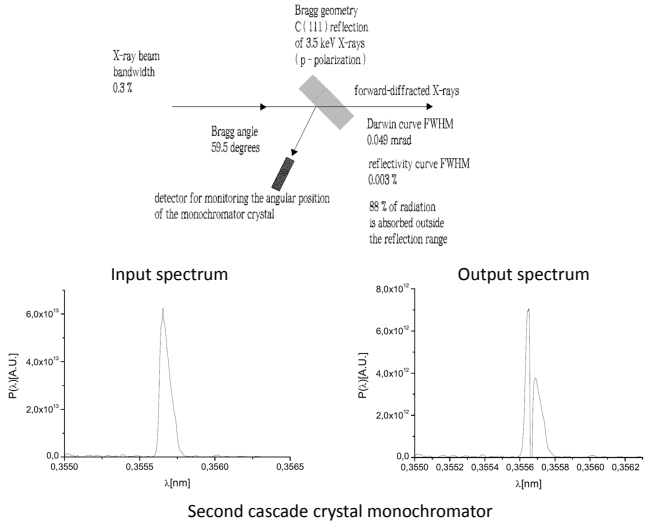

Fig. 6. Effect of the filtering process provided by the second diamond crystal on the incident spectrum of the radiation.

the incident angle and the spectral contents of the incoming beam satisfy the Bragg diffraction condition, the temporal waveform of the transmitted radiation pulse shows a long monochromatic wake, whose particular shape is linked to the shape of the filter in the frequency domain. The overall duration of this wake is inversely proportional to the bandwidth of the absorption line in the transmittance spectrum, while the particular shape of the wake, which in our case exhibits several oscillations on a shorter temporal scale, is due to the particular characteristics of the filter in the frequency domain. These characteristics are calculated in the frequency domain with the help of the dynamical theory of X-ray diffraction. In other words, all the physics involved can be limited to the frequency domain. After this task is accomplished, the particular shape of the wake can be simply interpreted as a consequence of a Fourier transform. It should be noted that, for the energy range under examination, between 3 keV and 5 keV, it is useful to consider the π-polarization of the C(111) reflection from a 0.1 mm-thick diamond crystal. The advantage of using the π-polarization is

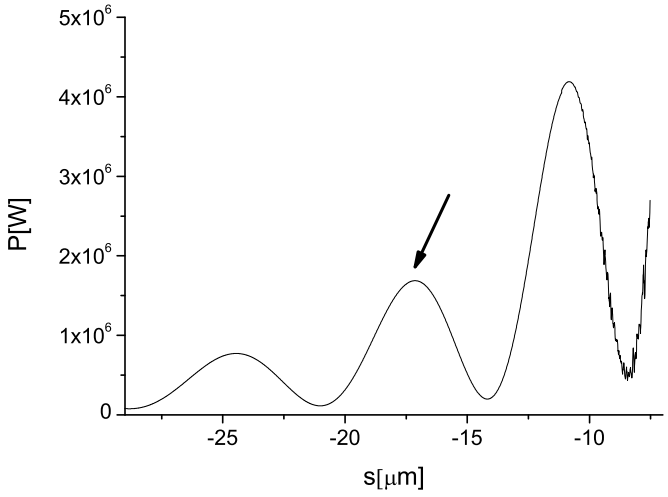

Fig. 7. Temporal shape of the seed signal from the second self-seeding setup. The black arrow indicates the seeding region used in this article.

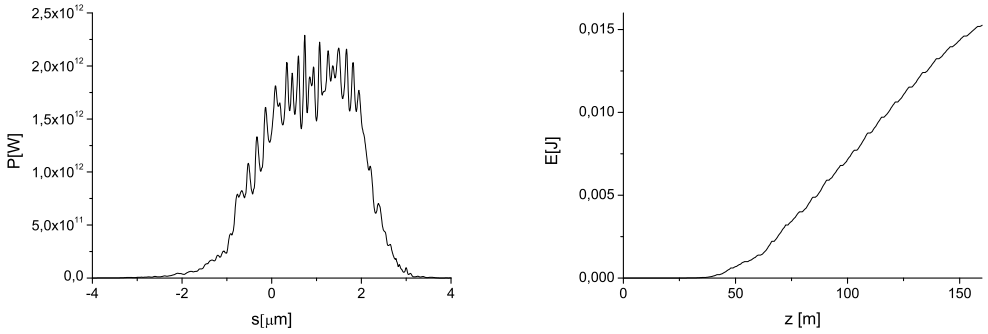

Fig. 8. (Left) The seeded FEL signal in the time domain after the tapered output undulator. (Right) Energy of the seeded FEL pulse as a function of the distance inside the output undulator.

due to the fact that the bandwidth of the reflectance is a few times narrower than for the σ-polarization in the entire energy range. As a result, the profile of the transmitted intensity in the time-domain appears more suitable for the temporal windowing operation, especially if one is interested in nearly Fourier-limited pulses.

While the radiation is sent through the crystal, the electron beam passes through a magnetic chicane, which accomplishes three tasks by itself: it creates an offset for the crystal installation, it removes the electron micro-bunching produced in the first undulator, and it acts as a delay line for the implementation of the temporal windowing. In other words, the magnetic chicane shifts the electron bunch on top of the monochromatic wake created by the bandstop filter thus selecting a part of the wake. This operation

amounts to a temporal windowing process. By this, the electron bunch is seeded with a radiation pulse characterized by a bandwidth much narrower than the natural FEL bandwidth. The temporal shape of the seed signal is shown in the left plot of Fig. 4, while the seeded FEL signal before the second self-seeding setup is shown in the right plot of the same figure.

For the hard X-ray wavelength range, a small dispersive strength R_{56} in the order of ten microns is sufficient to remove the micro bunching in the electron bunch. It is important to realize that the uncorrelated energy spread induced by quantum diffusion during the passage through the undulator is more than sufficient to wash-out the microbunching. In our case of interest, the energy spread induced by quantum diffusion always exceeds 1 MeV [2]. It should be remarked that this effect is of fundamental nature, and that the energy-spread so produced follows a Gaussian distribution. Based on this fact, the energy and density modulations will be damped following an exponential factor given by $\exp[- < (\delta\gamma)^2 > R_{56}^2/(2\gamma^2 \lambda\!\!\!^{-2})]$, where $< (\delta\gamma)^2 > /\gamma^2$ is the variance of the relative energy spread, R_{56} is the dispersion strength of the chicane, and $\lambda\!\!\!^{-}$ is the reduced wavelength. Considering a wavelength $\lambda = 0.35$ nm, an electron energy of 17.5 GeV, an $R_{56} \sim 30$ μm and, conservatively, an energy spread induced by quantum diffusion of 1 MeV, we obtain an enormously small exponential damping factor.

As a result of this discussion, the choice of the strength of the magnetic chicane only depends on the delay that we want to introduce between electron bunch and radiation. In our case, this amounts to 17 μm for the short pulse mode of operation. Such dispersion strength is small enough to be generated by a short 5 m-long chicane to be installed in place of a single undulator module. Such chicane is, however, strong enough to create a sufficiently large transverse offset of a few millimeters for installing the crystal.

The main problem in having crystal monochromators working between 3 keV and 5 keV is related with the low throughput due to absorption. In fact, about 88% of the radiation out of the reflection range is absorbed, resulting in low seeding power. The seed power level can be increased, to some extent, by making the first part of the undulator longer. This increases the signal-to-noise ratio. However, successful operation of the self-seeded XFEL requires operation of the first part of the undulator in the deep linear regime, and not in saturation. In fact, the amplification process in the FEL leads to an energy modulation in the electron beam. After the electron beam passes through the magnetic chicane, such energy modulation transforms

[2] In this article we discuss about SASE3 type undulators placed behind SASE1, which induces a relatively high energy spread in electron bunch due to quantum diffusion, definitely exceeding 1 MeV at the nominal energy of 17.5 GeV.

into additional energy spread.

The use of a second monochromator cascade enhances the signal-to-noise ratio without spoiling the electron beam quality. This enhancement is the consequence of the fact that the radiation pulse impinging on the second crystal is nearly Fourier-limited, meaning that there is an improvement of the bandwidth ratio of the signals before the first cascade (SASE) and the second cascade (seeded). This fact can be easily seen by comparing the spectral widths in Fig. 3 and Fig. 6, resulting in an increase of about a factor 5. Note that the power level before the first and the second cascade are roughly the same, and amount to about 1 GW, Fig. 5. Therefore, the improvement of the bandwidth ratio directly translates into an in improvement of the seed power (compare Fig. 4 and Fig. 7) of the same amount. The power level in Fig. 5 is much smaller than the power at saturation, which reaches about 100 GW, so that the electron beam is not significantly perturbed.

This fact is confirmed by simulations. In fact, the seed signal is finally amplified through the output undulator, which is tapered in order to optimize the exchange between electron energy and radiation (see the next section for details). The FEL signal from the entire setup is shown in the left plot of Fig. 8, which also includes a plot of the energy in the FEL pulse as a function of the distance inside the output undulator. As one can see, for this particular run one reaches about 2 TW output power.

If one wants to reach the same seed power with a single cascade, one needs to increase the power at the exit of the first undulator up to about 5 GW, thus perturbing the electron beam more. Simulations show that due to electron beam perturbations, in this case one cannot reach the same final output level of 2 TW.

3 FEL studies

With reference to Fig. 1 we performed feasibility studies pertaining the energy range considered in this article. These studies were performed with the help of the FEL code GENESIS 1.3 [28] running on a parallel machine. Simulations are based on a statistical analysis consisting of 100 runs.

The main undulator parameters are reported in Table 1. The electron beam characteristics at the entrance of the setup are summarized in Fig. 9, where we plot the results of start-to-end simulations [29].

First, the electron beam passes through the first part of the undulator and lases as a SASE source. The power and the spectrum after this first undulator,

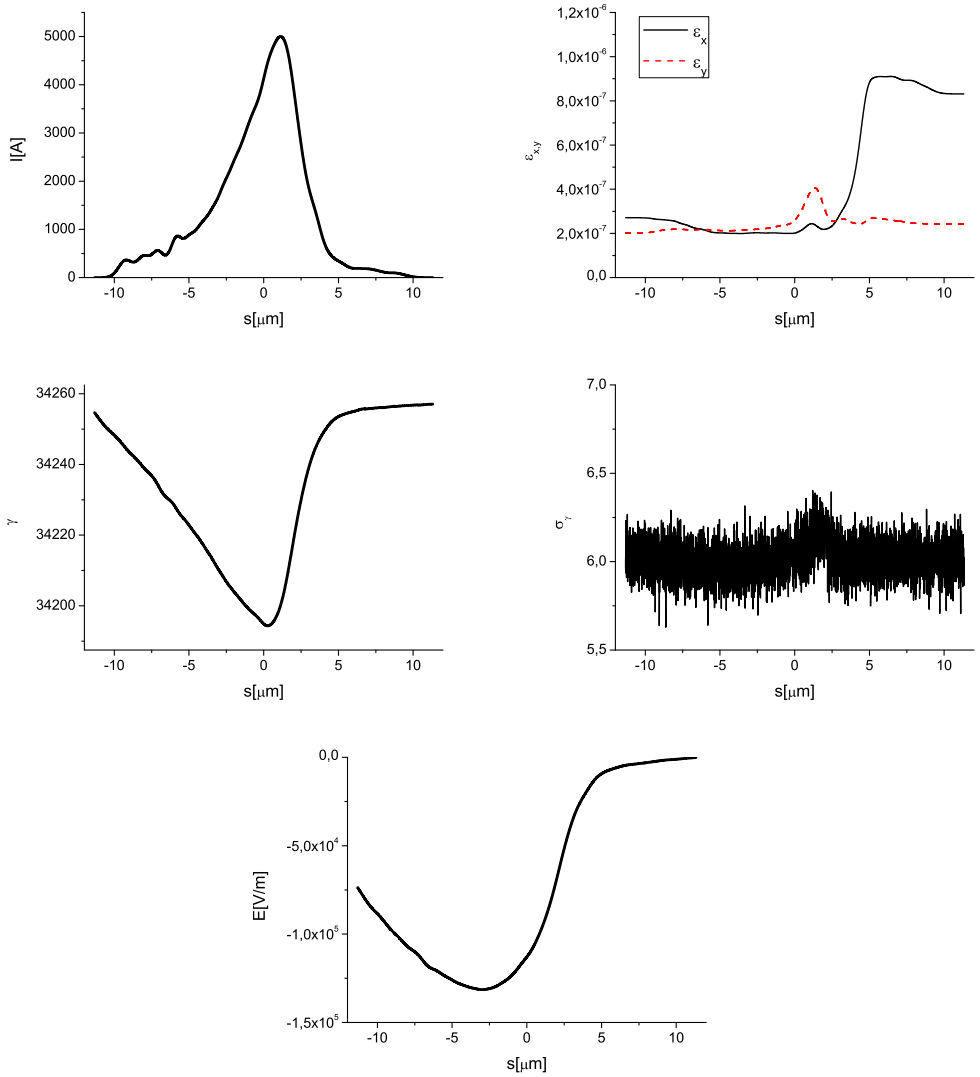

Fig. 9. Results from electron beam start-to-end simulations at the entrance of SASE3 [29] for the hard X-ray case. (First Row, Left) Current profile. (First Row, Right) Normalized emittance as a function of the position inside the electron beam. (Second Row, Left) Energy profile along the beam, lower curve. The effects of resistive wakefields along SASE1 are illustrated by the comparison with the upper curve, referring to the entrance of SASE1 (Second Row, Right) Electron beam energy spread profile, upper curve. The effects of quantum diffusion along SASE1 are illustrated by the comparison with the lower curve, referring to the entrance of SASE1. (Bottom row) Resistive wakefields in the SASE3 undulator [29].

and before the first self-seeding monochromator setup are shown in Fig. 10. This photon pulse passes through the first crystal acting as a band-stop filter as described before.

The results in frequency and time domain are shown in Fig. 11, where the trailing radiation pulse in the time-domain, due to the presence of the

Table 1
Undulator parameters

	Units	
Undulator period	mm	68
Periods per cell	-	73
Total number of cells	-	40
Intersection length	m	1.1
Photon energy	keV	3-5

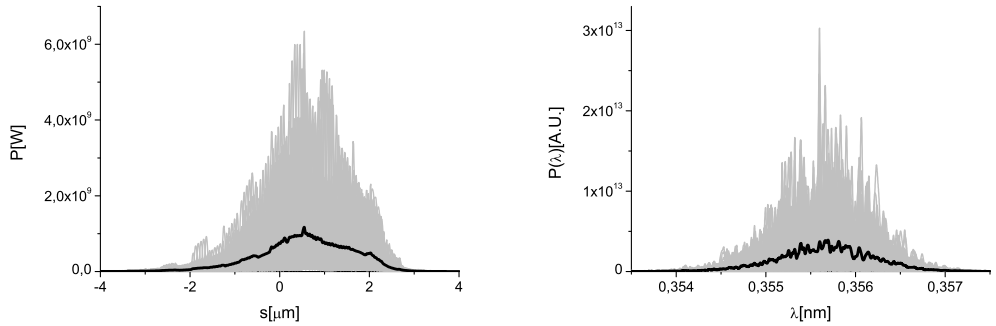

Fig. 10. Power and spectrum before the first hard X-ray self-seeding monochromator setup. Grey lines refer to single shot realizations, the black line refers to the average over a hundred realizations.

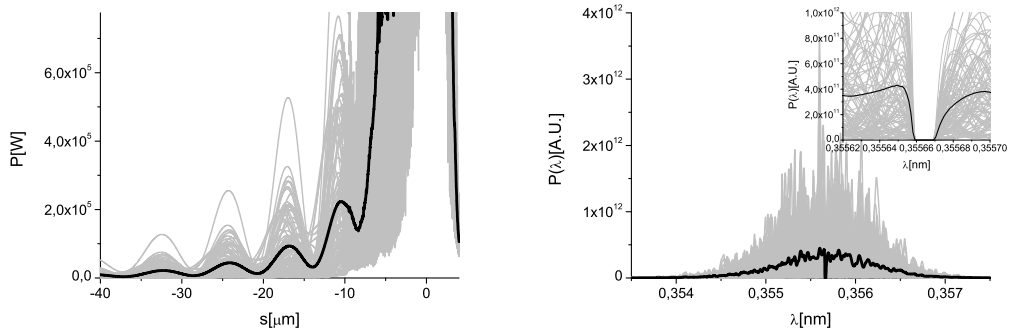

Fig. 11. Power and spectrum after the first hard X-ray self-seeding monochromator setup. Grey lines refer to single shot realizations, the black line refers to the average over a hundred realizations.

monochromator, is evident.

The electron beam modulations are washed-out by passing through the chicane, and is seeded with the trailing radiation pulse, which is then amplified in the second undulator part. The power and the spectrum of the radiation after the second part of the undulator is shown in Fig. 13.

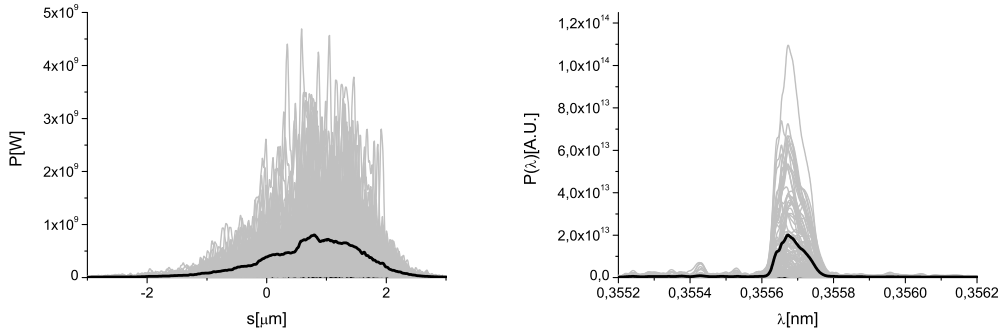

Fig. 12. Power and spectrum before the second hard X-ray self-seeding monochromator setup. Grey lines refer to single shot realizations, the black line refers to the average over a hundred realizations.

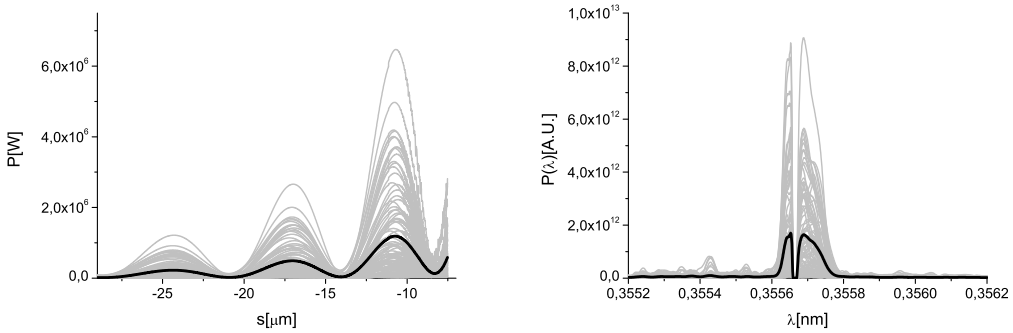

Fig. 13. Power and spectrum after the second hard X-ray self-seeding monochromator setup. Grey lines refer to single shot realizations, the black line refers to the average over a hundred realizations.

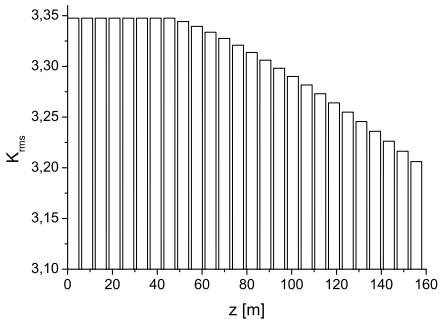

Fig. 14. Tapering law.

At this point the radiation pulse passes through the second monochromator setup. The fact that it is nearly Fourier limited allows a betterment of the signal-to-noise ratio of a large factor $\Delta\omega_{\mathrm{SASE}} \cdot \sigma_T$. This helps in countering the high absorption in the crystal. Fig. 13 shows the power and the spectrum after the second monochromator station.

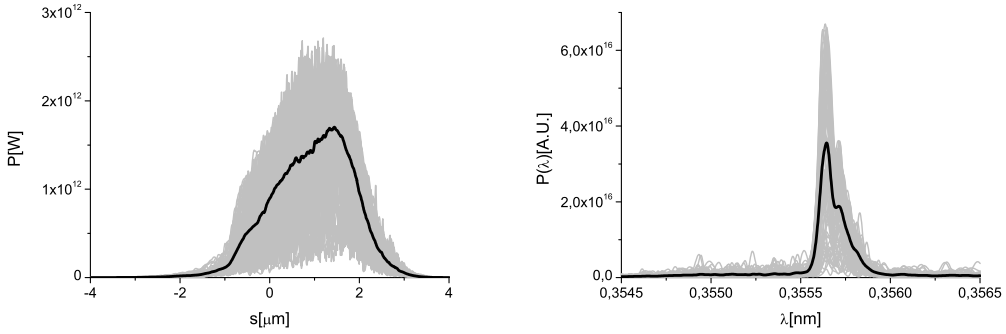

Fig. 15. Final output in the case of tapered output undulator for $\lambda = 0.35$ nm. Power and spectrum are shown. Grey lines refer to single shot realizations, the black line refers to the average over a hundred realizations.

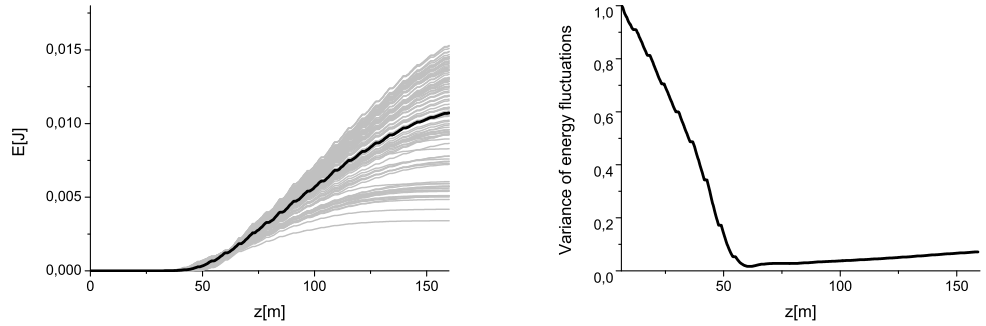

Fig. 16. Energy and energy variance of output pulses in the case of tapered output undulator for $\lambda = 0.35$ nm. In the left plot, grey lines refer to single shot realizations, the black line refers to the average over a hundred realizations.

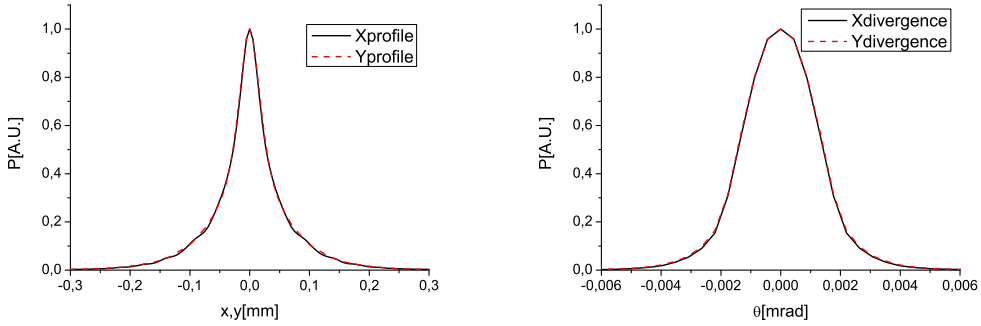

Fig. 17. Final output. X-ray radiation pulse energy distribution per unit surface and angular distribution of the X-ray pulse energy at the exit of output undulator for the case $\lambda = 0.35$ nm.

The electron beam finally goes through the output undulator, which is tapered according to the law shown in Fig. 14. Fig. 15, Fig. 16 and Fig. 17 show the output from the entire setup. Fig. 15 demonstrates that nearly Fourier-limited pulses with a power level of about 2 TW can be reached by

tapering the output undulator. Fig. 16 shows the energy and the variance of the radiation pulses as a function of the position inside the undulator. Finally, size and divergence of the X-ray pulses are plotted in Fig. 17.

4 Conclusions

A self-seeding scheme based on single crystal monochromator has been demonstrated experimentally and successfully compared with simulations [30]. Self-seeding is an excellent method for generating both monochromatic X-rays and high power pulses. Up to now, all studies have focused on operation in the hard X-ray energies (between 7 keV and 13 keV). However, future setups may need to be operated at lower energies. The interest in biomolecular imaging now includes also sources between 3 keV and 5 keV, and self-seeding schemes began to cope with this energy range [23]. In this paper we demonstrated the flexibility of our self-seeding scheme with single crystal monochromator to cover a wide photon energy range. This kind of operation is easily achieved with diamond crystals in symmetric Bragg reflection geometry. In particular, based on the use C(400), C(220), and C(111) reflections it will be possible to cover photon energy range from 13 keV down to 3.5 keV. Therefore, this extremely compact self-seeding scheme is ideally suited for bio-imaging applications. In this paper we proposed a study of the performance of the self-seeding scheme with single crystal monochromator for the European X-ray FEL at X-ray energies lower than 5 keV. By combining the two techniques of cascade self-seeding and undulator tapering we found that 2 TW X-ray, nearly transform-limited pulses down to photon energy range 3.5 keV can be generated from baseline-scale 40 cells undulators.

5 Acknowledgements

We are grateful to Massimo Altarelli, Reinhard Brinkmann, Henry Chapman, Janos Haidu, Viktor Lamzin, Serguei Molodtsov and Edgar Weckert for their support and their interest during the compilation of this work.

References

[1] J. Hajdu, Curr. Opin. Struct. Biol. 10, 569 (2000)
[2] R. Neutze et al., Nature 406, 752 (2000)
[3] K. J. Gaffney and H. N. Chapman, Science 316, 1444 (2007)

[4] A. Lin and J.M. Dawson, Phys. Rev. Lett. 42 2172 (1986)
[5] P. Sprangle, C.M. Tang and W.M. Manheimer, Phys. Rev. Lett. 43 1932 (1979)
[6] N.M. Kroll, P. Morton and M.N. Rosenbluth, IEEE J. Quantum Electron., QE-17, 1436 (1981)
[7] T.J. Orzechovski et al., Phys. Rev. Lett. 57, 2172 (1986)
[8] W. Fawley et al., NIM A 483 (2002) p 537
[9] M. Cornacchia et al., J. Synchrotron rad. (2004) 11, 227-238
[10] X. Wang et al., PRL 103, 154801 (2009)
[11] J. Feldhaus et al., Optics. Comm. 140, 341 (1997).
[12] E. Saldin, E. Schneidmiller, Yu. Shvyd'ko and M. Yurkov, NIM A 475 357 (2001).
[13] E. Saldin, E. Schneidmiller and M. Yurkov, NIM A 445 178 (2000).
[14] R. Treusch, W. Brefeld, J. Feldhaus and U Hahn, Ann. report 2001 "The seeding project for the FEL in TTF phase II" (2001).
[15] A. Marinelli et al., Comparison of HGHG and Self Seeded Scheme for the Production of Narrow Bandwidth FEL Radiation, Proceedings of FEL 2008, MOPPH009, Gyeongju (2008).
[16] G. Geloni, V. Kocharyan and E. Saldin, "Scheme for generation of highly monochromatic X-rays from a baseline XFEL undulator", DESY 10-033 (2010).
[17] Geloni, G., Kocharyan V., and Saldin, E., "A novel Self-seeding scheme for hard X-ray FELs", Journal of Modern Optics, vol. 58, issue 16, pp. 1391-1403, DOI:10.1080/09500340.2011.586473 (2011)
[18] G. Geloni, V. Kocharyan and E. Saldin, "Scheme for generation of fully coherent, TW power level hard x-ray pulses from baseline undulators at the European XFEL", DESY 10-108 (2010).
[19] Geloni, G., Kocharyan, V., and Saldin, E., "Production of transform-limited X-ray pulses through self-seeding at the European X-ray FEL", DESY 11-165 (2011).
[20] W.M. Fawley et al., Toward TW-level LCLS radiation pulses, TUOA4, to appear in the FEL 2011 Conference proceedings, Shanghai, China, 2011
[21] J. Wu et al., Simulation of the Hard X-ray Self-seeding FEL at LCLS, MOPB09, to appear in the FEL 2011 Conference proceedings, Shanghai, China, 2011
[22] Y. Jiao et al. Phys. Rev. ST Accel. Beams 15, 050704 (2012)
[23] G. Geloni, V. Kocharyan and E. Saldin, "Conceptual design of an undulator system for a dedicated bio-imaging beamline at the European X-ray FEL", DESY 12-082 (2012)
[24] I Ben-Zvi and L. H. Yu, Nucl. Instr. and Methods, A 393, 96 (1997).
[25] Y. Feng, J. Hastings, P. Heimann, M. Rowen, J. Krzywinski, and J. Wu, "X-ray Optics for soft X-ray self-seeding the LCLS-II", proceedings of 2010 FEL conference, Malmo, Sweden, (2010).
[26] Y. Feng, P. Heimann, J. Wu, J. Krzywinski, M. Rowen, and J.

Hastings, "Compact Grating Monochromator Design for LCLS-I Soft X-ray Self-Seeding", https://slacportal.slac.stanford.edu/sites/lcls_public/lcls_ii/Lists/LCLS_II_Calendar/Physics_Meetings.aspx, May 2011 and https://sites.google.com/a/lbl.gov/realizing-the-potential-of-seeded-fels-in-the-soft-x-ray-regime-workshop/talks, October 2011

[27] G. Geloni, V. Kocharyan and E. Saldin, "A Cascade self-seeding scheme with wake monochromator for narrow-bandwidth X-ray FELs", DESY 10-080 (2010).

[28] S Reiche et al., Nucl. Instr. and Meth. A 429, 243 (1999).

[29] I. Zagorodnov, "Beam Dynamics Simulations for XFEL", http://www.desy.de/xfel-beam/s2e (2011).

[30] P. Emma, Hard X-ray Self-seeding at the Linac Coherent Light Source, Proceedings of the IPAC 2012 Conference, New Orleans, USA (2012).